Tomographic optoacoustic inversion in dynamic illumination scenarios

Thomas Jetzfellner[a], Amir Rosenthal[a], Andreas Buehler[a], Alexander Dima[a], Karl-Hans Englmeier[a], Vasilis Ntziachristos[a], and Daniel Razansky[a],*

[a]Institute for Biological and Medical Imaging (IBMI), Technische Universität München and Helmholtz Zentrum München, Ingolstaedter Landstr. 1, 85764 Neuherberg, Germany

ABSTRACT

Obtaining quantified optoacoustic reconstructions is an important and longstanding challenge, mainly caused by the complex heterogeneous structure of biological tissues as well as the lack of accurate and robust reconstruction algorithms. The recently introduced model-based inversion approaches were shown to eliminate some of reconstruction artifacts associated with the commonly used back-projection schemes, while providing an excellent platform for obtaining quantified maps of optical energy deposition in experimental configurations of various complexity. In this work, we introduce a weighted model-based approach, capable of overcoming reconstruction challenges caused by per-projection variations of object's illumination and other partial illumination effects. The universal weighting procedure is equally shown to reduce reconstruction artifacts associated with other experimental imperfections, such as non-uniform transducer sensitivity fields. Significant improvements in image fidelity and quantification are showcased both numerically and experimentally on tissue phantoms.

Keywords: Optoacoustic Imaging, Inversion Schemes, Light Diffusion

1. INTRODUCTION

Optoacoustic tomography (OAT) is a fast evolving non-invasive imaging method for high resolution mapping of optical absorption in tissues [1-4]. The imaging is performed by illuminating the object or region of interest with a short high-power laser pulses, thus creating an instantaneous temperature elevation and thermal expansion within it. The resulting broadband ultrasonic waves (typically in the 0.1–10 MHz range) carry information on the underlining optical absorption coefficient variations, local light fluence, and thermoelastic properties of the object. By tomographically collecting optoacoustic responses around the object and using optoacoustic inversion algorithms [2, 5-7] one can reconstruct an image representing local laser energy deposition within the object.

In contrast to conventional ultrasound imaging, attaining relatively low contrast between different soft tissues, optoacoustic tomography visualizes the optical contrast, which is significantly richer in distinguishing different tissues and biomarkers, including oxygenated and deoxygenated forms of hemoglobin or endogenously or extrinsically administered absorbers. Additionally, due to weak scattering of ultrasonic waves in biological tissues, the resolution is similar to that achieved with ultra-sonography i.e. it can reach 20- 200 microns depending on the penetration depth and corresponding frequency spectrum used. By combining therefore optical contrast with ultrasonic diffraction-limited resolution optoacoustics holds a great promise for future biomedical applications. Besides intrinsic measurements of morphology and disease-related vascular changes [8-10], various contrast media approaches have been also developed for enhancement of detection sensitivity and specificity of the method, including dyes [11], light-absorbing nano-particles [12], and chromogenic substrates [13]. More recently, by applying illumination at several optical wavelengths, multispectral optoacoustic tomography (MSOT) was able to resolve distribution of fluorescent molecular agents [14] and fluorescent proteins [15] with both high sensitivity and spatial resolution in optically opaque organisms and tissues.

OAT reconstructions are usually very sensitive to various instrumentation and configuration-related parameters, such as the shape of object's illumination, transducer layout, its frequency response and sensitivity fields, as well as laser source stability. Many approximated inversion schemes, including the commonly used back-projection algorithms [7], are not suitable for accurately describing the optoacoustic tomographic problem. If these deviations become substantial,

Photons Plus Ultrasound: Imaging and Sensing 2011, edited by Alexander A. Oraevsky, Lihong V. Wang,
Proc. of SPIE Vol. 7899, 78991Y · © 2011 SPIE · CCC code: 1605-7422/11/$18 · doi: 10.1117/12.876110

unquantified or generally erroneous reconstructions may arise. It was shown that variety of configuration-related parameters could be taken into account when using exact model-based reconstruction schemes [16] . With the recent introduction of numerically efficient interpolated-model-matrix inversion (IMMI) [5], these methods are no longer afflicted with long computation times.

When considering the effects of object illumination, optoacoustic image quality and quantification abilities normally depend on homogeneity and uniformity of excitation light distribution. This is especially important in cases of varying illumination, e.g. when the imaged object is rotated with respect to both illumination and ultrasound detection elements [17]. In an ideal optoacoustic tomography scenario, the imaged region shall be illuminated as uniformly as possible, which can be achieved by e.g. expanding the laser beam to an appropriate width to cover the entire object. However, this solution is only suitable if the laser power is strong enough so that an appropriate signal-to-noise (SNR) ratio can be attained after beam widening. Yet, even if the laser power is too weak for these optimal illumination conditions, the object can still be imaged by partially illuminating it. Overall, in many realistic imaging cases, where large parts of the object are not accessible for light or its geometry is not suitable for uniform illumination, a sub-optimal partial illumination arrangement is the only method to actually perform optoacoustic imaging at the expense of reduced tomographic quality of the data. Similar issues are arising regarding the sensitivity fields of the transducers used for optoacoustic detection. These are generally not homogenous and have strong dependence not only on the distance from the detector but also on the detection angle [18].

Herein we present a weighted model-based reconstruction algorithm, which is based on integrating an approximated light-fluence model in the optoacoustic forward model by weighting the elements in the model matrix. Our main focus here is on light-related reconstruction effects, however, the proposed method can equally be used in other scenarios, e.g. for spatially dependant sensitivity which varies for different positions of the acoustic detector. Improvements in the image fidelity and quantification are demonstrated based on both numerical simulations and experiments using realistic tissue-mimicking phantoms and mice.

2. BACKGROUND

It has been previously shown that model-based reconstruction approach can be readily generalized to include linear effects that characterize the optoacoustic imaging system. Specifically, in Ref [5] the frequency response of the detector was taken into account by assuming it did not vary significantly within the imaged region. Thus, in that generalization, the sensitivity of the detector to each point in the imaged object was assumed to be the same. While this first order approximation yielded good initial results, in many scenarios the spatial variations in object's illumination and detection sensitivity are too large to be neglected, thus requiring additional modeling.

A typical example of imaging configuration, in which modeling the spatially-dependant sensitivity is crucial, occurs when the illumination differs for each projection [19] (Fig. 1a). While uniform illumination is considered to be the best theoretical choice, it might not be practical due to technical constraints. For instance, if the laser power is not sufficiently strong, expanding the beam to allow uniform illumination of the imaged object will decrease the beam's intensity, readily resulting in lower SNR, reduced image quality or significantly prolonged reconstruction times due to signal averaging. Since in many practical cases not all of the generated optoacoustic fields are detected simultaneously, the SNR can be significantly improved by illuminating only the parts of the object that are best detected in each particular projection of the imaging geometry.

Similar considerations apply to the ultrasonic detection part. Spatial dependence is a common attribute of conventional acoustic transducers used for optoacoustic detection. Generally, the dependence is not only upon the distance from the detector but also on the detection angle [18]. This dependence can be mitigated by placing the transducer farther from the sample, however, such a solution comes on the expense of SNR. Thus, similarly to the case of non-uniform illumination, there is a tradeoff between uniform sensitivity and maximum sensitivity, which might result in a limited view acoustic detection scenario (Fig. 1b).

In some cases, incomplete tomographic data is obtained due to both partial illumination and limited-view or focused acoustic detection. A typical example is the dark-field photoacoustic microscopy (PAM) [20] where both illumination and sound detection are confined to a relatively small focal region, which is also translated along the object's surface in order to capture three-dimensional image data (Fig. 1c).

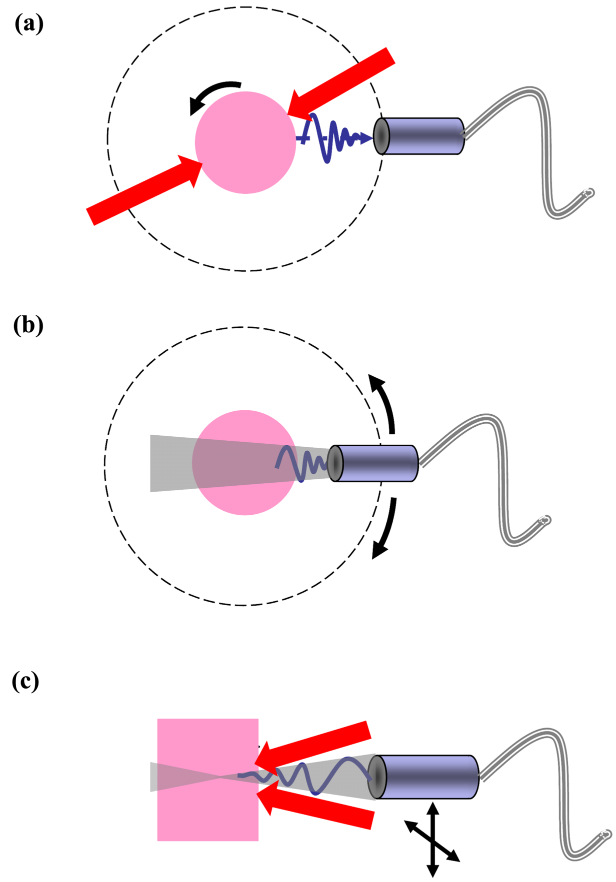

Figure 1: Optoacoustic imaging configurations with partial or variable tomographic data. (a) Circular scanning with narrow laser beam and a rotating object. Illumination and detector are static; (b) Circular scanning with ultrasonic detector having limited angular view. The imaged object and illumination are static; (c) Optoacoustic microscopy (B-mode) imaging with confocal illumination-detection geometry and linear translation.

An additional spatially-dependent effect is acoustic attenuation. Because acoustic attenuation depends on the distance of the source from the detector, its effect may be different for different regions in the imaged specimen. This effect may become significant in imaging relatively large animal such as mice and when imaging fatty tissue, which has a relatively high attenuation coefficient [21].

3. THEORY

The optoacoustic effect involves the creation of acoustic waves in an optically opaque medium originating from instantaneous thermal expansion induced by the absorption of short light pulses in the medium [3]. Optoacoustic tomography (OAT) maps the optical absorption of tissue by illuminating its surface and measuring the emitted optoacoustic responses in a tomographic setup. Typical light pulses used in OAT have durations below 10ns, which fulfill both thermal and stress confinement condition thus are sufficiently short to be approximated by a temporal delta function. In this case, under the assumption of an acoustically homogeneous medium, the pressure field distribution at any given location and time can be expressed via Poisson-type integral [5]

$$p(r,t)=\frac{\Gamma}{4\pi c}\frac{\partial}{\partial t}\int_{R=ct}\frac{H_r(r')}{R}dA', \tag{1}$$

where c and Γ are velocity of sound and Grüneisen parameter of tissue, H_r represents spatial distribution of the absorbed energy within the imaged object. The integration in Eq. 1 is performed over a sphere in the three-dimensional case and over a circle in the two-dimensional case, both having a radius of $R=|r-r'|=ct$.

Inverting the relation in Eq. 1 can yield $H_r(r)$ within the imaged object from the acoustic fields measured at a discrete set of points $\{r_k\}$. The inversion can be performed using analytical solutions, such as back-projection algorithms, or model-based solutions, which are based on direct numerical solutions to Eq. 1. In Ref. [5], Eq. 1 was solved by applying linear interpolation to $H_r(r)$ and performing the integral analytically. This leads to a discretization of Eq. 1, given by the following matrix relation

$$p^k=\mathbf{M}^k z, \tag{2}$$

Where p^k is a column vector representing the acoustic fields measured at a position (projection) r_k (k=1…K), for a set of times $\{t_i\}$ (i=1…I): $p_i^k=p(r_k,t_i)$; z is a column vector representing the values of the optoacoustic image on the grid $z_j=H(r_j)$ (j=1:…J); and M^k is the acoustic forward-model matrix for a detector at r_k.

The set of K matrix equations given in Eq. 2, can be written as a single matrix equation by stacking the vectors and matrices. This leads to the following matrix relation:

$$p=\mathbf{M}z, \tag{3}$$

where $p=[p_1^t,p_2^t,...,p_k^t]^t$ and $\mathbf{M}=[\mathbf{M}_1^t,\mathbf{M}_2^t,...,\mathbf{M}_k^t]^t$, where t denotes the transpose operation.

In order to obtain the optoacoustic image, Eq. 3 needs to be inverted. Two common methods are the Moore-Penrose pseudo-inverse [22] and the LSQR (least squares QR decomposition) algorithm [23] .The pseudo-inverse of **M** is given by

$$\mathbf{M}^+=(\mathbf{M}^H\mathbf{M})^{-1}\mathbf{M}^H, \tag{4}$$

After the pseudo-inverse is calculated, the reconstructed optoacoustic image can then be readily obtained:

$$z=\mathbf{M}^+p, \tag{5}$$

The main advantage of using the pseudo-inverse is that it needs to be calculated for a given system only once. Thus, if the pseudo-inverse is pre-calculated, the inversion can be performed in real time.

LSQR is an iterative algorithm for solving linear equations [23]. Analytically, LSQR is identical to the conjugate gradient method. However, numerically LSQR was found to be more stable. The main advantage of LSQR is its high efficiency in the case of sparse matrices. In addition, the operation performed in LSQR require saving only the non-zero elements of the matrix in memory, thus mitigating memory requirements. Since the model matrix **M** is sparse [5], LSQR is an extremely efficient method for inverting Eq. 3 when the number of grid points is high.

The function $H_r(r)$ represents the total amount of optical energy transferred to the imaged object from a single light pulse at a point r, and is given by

$$H(r) = \mu_a(r)U(r), \tag{6}$$

where $\mu_a(r)$ is the absorption coefficient and $U(r)$ is the light fluence. To model the light fluence, we assumed diffusion approximation to light transport equation [24], i.e.

$$-\nabla D(\vec{r})\nabla U(\vec{r}) + \mu_a(\vec{r})U(\vec{r}) = q_0, \tag{7}$$

where $D = 1/[3(\mu_s' + \mu_a)]$ is the spatially dependent diffusion coefficient of the medium, U is the light intensity, μ_a is the optical absorption coefficient, μ_s' is the reduced scattering coefficient and q_0 is the source term. When the exterior medium is non-scattering, the behavior of $U(r)$ on the interface is given by the Robin boundary condition [25]:

$$U(\vec{r}) + 2D(\vec{r})\hat{\mathbf{n}} \cdot \nabla \cdot U(\vec{r}) = 0 \qquad \vec{r} \in \partial\Omega \tag{8}$$

where $\partial\Omega$ is the boundary of the object and $\hat{\mathbf{n}}$ is a unit vector normal to $\partial\Omega$ and pointing outwards. Clearly, for heterogeneous media, solutions for Eq. (8) can only be obtained numerically. In our work, we used a finite volume method (FVM) solution approach [26].

When the spatially-dependant sensitivity of the detection is known, it can be incorporated into the model matrix of IMMI by weighting its elements. Denoting the weight function by $W^k(r)$, the weighted model-matrix elements are given by

$$\breve{\mathrm{M}}_{ij}^k = W^k(r_j)\breve{\mathrm{M}}_{ij}^k, \tag{9}$$

where r_j are the location of the grid points. The matrices $\breve{\mathrm{M}}^k$ $(k=1...K)$ can be used to construct the total weighted matrix $\breve{\mathrm{M}} = [\breve{\mathrm{M}}^1, \breve{\mathrm{M}}^2, ..., \breve{\mathrm{M}}^K]$. The forward matrix M from Eq. (4) is then replaced with the weighted matrix $\breve{\mathrm{M}}$ and inverted by using either the Moore-Penrose pseudo-inverse equation (Eq. 4) or the LSQR algorithm.

In the case in which the illumination changes as a function of the position of the acoustic detector [19] (Fig. 1a), the weighting function can be numerically calculated. The optoacoustic image for the k-th position of the detector (projection) is given by

$$H^k(r) = \mu_a(r)U^k(r), \tag{10}$$

The optoacoustic image for each value of k can be presented as a function of the image in the case of uniform illumination:

$$H^k(r) = H(r)W^k(r), \tag{11}$$

where the weight function $W^k(r)$ is given by $W^k(r) = U^k(r)/U(r)$. In order to calculate $W^k(r)$, the light diffusion equation needs to be calculated twice: once for uniform illumination and once for the specific illumination pattern of the k-th projection. While the exact fluence pattern can only be calculated if the absorption and scattering coefficients are known, it can be approximated by using typical values for these coefficients. The approximation can be subsequently improved by using the reconstructed optoacoustic image to get a better estimate for the absorption coefficient and calculate $W^k(r)$ in iterations [24].

4. NUMERICAL EXPERIMENTS

In this section we numerically demonstrate the proposed reconstruction algorithm for the partial illumination configuration, shown in Fig. 1a. All the inversion algorithms were implemented in Matlab (Mathworks Inc., Natick, MA), and executed on an Intel® Core™2 Quad Processor CPU operating at 2.67GHz with 4 Gbyte of RAM. All the model-based reconstructions were obtained using LSQR for inversion.

We numerically tested our correction algorithm for a round tissue-mimicking phantom containing two square inclusions with higher absorption compared to the background. The bulk of the phantom was assigned an absorption coefficient of μ_a=0.2cm^{-1}, whereas the top and bottom insertions had absorption coefficients of 0.6 cm^{-1}, and 0.4 cm^{-1}, respectively. The scattering coefficient was chosen to be constant and had the value of 10 cm^{-1}. Figures 2a and 2b show the reconstructions obtained using standard IMMI [5] and the back-projection algorithm [7] assuming constant and uniform surface illumination and circular detection geometry with 180 projections. As expected, the model-based approach achieves an almost exact reconstruction, whereas the back-projection algorithm suffers from negative artifacts and does not correctly capture the effect of light attenuation, making the image non-quantitative.

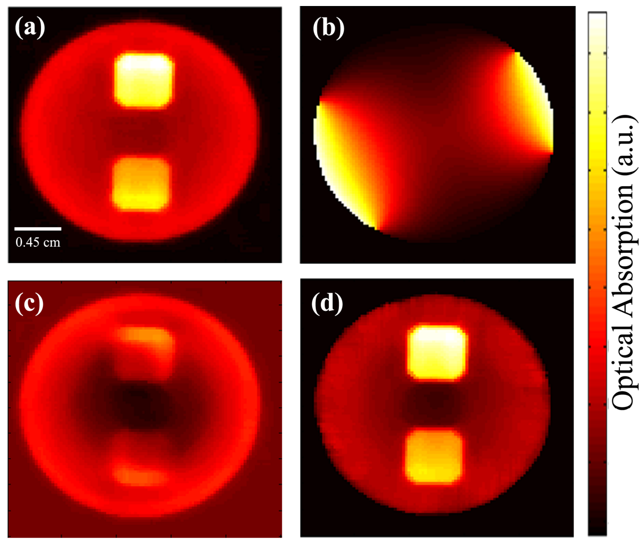

Figure 2: Reconstructions of numerical tissue-mimicking phantom for the homogeneous illumination case with (a) model-based (b) light propagation model used in the simulated partial illumination case for weighting and correction; (c) standard model-based reconstruction with partial illumination; (d) image corrected for partial illumination using the weighted model-based approach.

The non-uniform illumination was simulated using two beams coming at angles of 20° and 200° relative to the detector, and having widths of 0.75cm and 1 cm, respectively (Fig. 1a). We simulated the light beams and detector to encircle the imaged object with 2° increments to acquire a full optoacoustic tomographic data set. Figure 2b shows the light fluence for the projection in which the detector is positioned as in Fig. 1a (3 o'clock orientation). Clearly, over half the phantom's boundary is not illuminated. The reconstructions obtained using standard IMMI is shown in Fig. 2c, respectively. The accuracy of the model-based reconstruction significantly deteriorates as compared to Fig. 2a with loss of contrast and blurring artifacts.

In order to correct for the non-uniform illumination, the fluence ought to be approximated for both the non-uniform and uniform illumination geometries. Since the exact map of optical absorption distribution is not a priori known in optoacoustic experiments, the light diffusion equation was solved for a phantom with estimated background absorption and scattering coefficients: μ_a=0.2cm^{-1}, μ_s'=10cm^{-1}. The illumination profile, which can be measured experimentally, was modeled exactly according to the one used to generate the optoacoustic data. The approximated fluences were used to calculate weight function $W^k(r)$, which was incorporated into the model using Eqs. 9-11. The reconstruction obtained using weighted IMMI is shown in Fig. 2d. Despite the rough estimation of the optical properties used for modeling of light propagation, the corrected image shows a significant improvement in the reconstruction quality, which is comparable to the one obtained for uniform illumination (Fig. 2a).

5. EXPERIMENTAL VALIDATION

In addition to the numerical demonstration, we have experimentally verified performance of the weighted inversion method on tissue mimicking phantoms. The measurements were performed in a tomographic continuous acquisition scanner [19]. Briefly, a tunable optical parametric oscillator laser (MOPO-710, Spectra-Physics, Mountain View, CA, USA), providing < 8 nsec duration pulses with 15 Hz repetition frequency in the visible spectrum (450–680 nm), was used in order to illuminate the sample under investigation. In all our experiments, we used a wavelength 650 nm which yielded an average power of approximately 450 mW. In ideal illumination conditions, the laser's beam was expanded to about 2 cm and split into two beams, thus creating a nearly uniform light pattern around the object. Subsequently, the beam size was reduced with focusing lenses to 0.8 cm in order to simulate the partial illumination scenario (Fig. 1a). A cylindrically focused transducer (Model V382, Panametrics-NDT, Waltam, MA), was used to record the optoacoustic signals emitted by the sample within the imaging plane. For collection of the signals over 360° projections, the samples were rotated on a stage while the transducer was placed at its focal distance of 38.1 mm from the center of rotation.

To showcase reconstruction improvements attained by the weighted model-based inversion, two phantoms were constructed. Both phantoms were cylindrically shaped and had a diameter of 16 mm, background absorption coefficient of $\mu_a' = 0.2$ cm^{-1} and reduced scattering coefficient of $\mu_s' = 10$cm^{-1}. The first one was used as an imaging target while the second phantom served for calibration of light deposition pattern on the surface of the imaged objects. For this, a thin carbon stick was embedded at the phantom's surface. By rotating the phantom, magnitudes of optoacoustic responses from the stick were recorded over 360^{o}.

The tomographic optoacoustic data were collected over 360 degrees with increments of 3 degrees. All the reconstructions were performed using 100×100 grid, which corresponded to pixel size of approximately 160 μm. The images of the phantom were first reconstructed for the full illumination case with laser beams covering the entire width of the phantom, as shown in Fig. 3a. The average values of the experimentally reconstructed absorption coefficient in the two insertions were 0.32 cm^{-1} and 0.41 cm^{-1}. Subsequently, the beam size was reduced to approximately 0.8 cm and the image reconstructed by the standard model-based inversion assuming uniform illumination (Fig. 3b). As expected, due to incorrect illumination assumptions and similarly to the numeric simulations, one can observe surface blurring effects while the other structures in the phantom's center are barely visible. To correct for these artifacts, we have used the illumination maps previously obtained with the calibration phantom. Eqs. 7-8 were utilized in order to build a weighted matrix for each projection, which was subsequently applied for obtaining the weighted forward model. The run time for constructing and inverting the model matrix was approximately 30 minutes for the given experimental setup. We used a sparse representation of the matrices and solved the inversion by using LSQR. The sparse matrix occupied approximately 1.5 GB of memory. The results of the weighted reconstruction are presented in Fig. 3c and clearly show that the method was able to correct for image artifacts introduced by the sub-optimal partial illumination. The average values of the reconstructed absorption coefficient in the two insertions were in this case 0.326 cm^{-1} and 0.42 cm^{-1}.
To demonstrate the stability of the algorithm we built the weights using different estimations of background absorption. The algorithm is stable for variations of +/- 0.1 cm^{-1} between the real background absorption and the one assumed in the model.

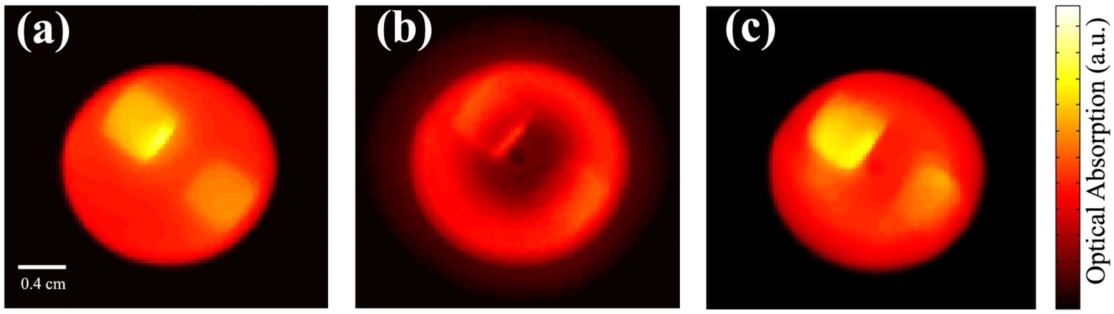

Figure 3. Model-based reconstruction for the a) Fully illuminated phantom; b) Variable partial illumination; c) Including weighting correction;

Apparently, the uniform illumination experiment attained a slightly better quantification as compared to the weighted model-based correction algorithm. The relatively small discrepancies can be attributed to inaccuracies in characterization of the beam and building the model. Clearly, the diffusion equation can only serve as an approximation to the realistic fluence distribution while possible inaccuracies in the positioning of the calibration phantom relatively to the reconstructed phantom could introduce additional errors. Nevertheless, the algorithm was shown to significantly improve overall image quality and quantification compared to the uncorrected image.

6. CONCLUSION

In this work, we presented a weighted version of the model-based inversion method for quantified optoacoustic tomography reconstructions. The algorithm is intended for correction of image artifacts associated with sub-optimal partial illumination and non-uniform acoustic detection fields.

The advanced semi-analytical model-based inversion scheme was successfully tested and compared to the unweighted model based reconstruction on both numerical and experimental data. For the simulated data, the weighted model based reconstruction and original image were almost identical. In contrast, similar correction using back-projection reconstruction is so far not possible thus quantification remains challenging due to intrinsic inaccuracies of the method in the form of negative values and erroneous accentuation of fast absorption variations in the image. For the numerical phantoms, the weighted model-based inversion was able to correct the blurring and smearing effects so that the shape and absorption values in the inclusions were nearly the same compared to the homogeneously illuminated phantoms. The corrected images in the experimental case showed deviations of below 10% from the real absorption values in the phantom.

The results attained by the proposed reconstruction method emphasize the advantages of the semi-analytical model-based inversion scheme over other commonly-used reconstruction methods for OAT. The methodology provides therefore a more generalized tomographic framework and serves as a robust method for quantitative optoacoustic image reconstruction.

REFERENCES

[1] A. A. Oraevsky, S. L. Jacques, R. O. Esenaliev *et al.*, "Laser based optoacoustic imaging in biological tissues," Proc. SPIE, 2134A, 122-128 (1994).

[2] R. A. Kruger, "Photoacoustic ultrasound (PAUS)—Reconstruction tomography," Medical Physics, 22(10), 1605 (1995).

[3] L. Wang, [Photoacoustic imaging and spectroscopy] CRC Press (2009).

[4] V. Ntziachristos, and D. Razansky, "Molecular Imaging by Means of Multispectral Optoacoustic Tomography (MSOT)," Chemical Reviews, 110(5), 2783-2794 (2010).

[5] A. Rosenthal, D. Razansky, and V. Ntziachristos, "Fast semi-analytical model-based acoustic inversion for quantitative optoacoustic tomography.," IEEE Trans Med Imaging, 29(6), 1275 - 1285 (2010).

[6] H. Jiang, Z. Yuan, and X. Gu, "Spatially varying optical and acoustic property reconstruction using finite-element-based photoacoustic tomography," Journal of the Optical Society of America A, 23(4), 878-888 (2006).

[7] M. Xu, and L. V. Wang, "Universal back-projection algorithm for photoacoustic computed tomography," Physical Review E, 71(1), (2005).

[8] J. Laufer, D. Delpy, C. Elwell *et al.*, "Quantitative spatially resolved measurement of tissue chromophore concentrations using photoacoustic spectroscopy: application to the measurement of blood oxygenation and haemoglobin concentration," Physics in Medicine and Biology, 52(1), 141-168 (2007).

[9] J. Jose, S. Manohar, R. G. M. Kolkman *et al.*, "Imaging of tumor vasculature using Twente photoacoustic systems," Journal of Biophotonics, 2(12), 701-717 (2009).

[10] L. Song, K. Maslov, and L. V. Wang, "Section-illumination photoacoustic microscopy for dynamic 3D imaging of microcirculation in vivo," Optics Letters, 35(9), 1482-1484 (2010).

[11] A. Buehler, E. Herzog, D. Razansky *et al.*, "Video rate optoacoustic tomography of mouse kidney perfusion," Opt Lett, 35(14), 2475-7 (2010).

[12] A. Taruttis, E. Herzog, D. Razansky *et al.*, "Real-time imaging of cardiovascular dynamics and circulating gold nanorods with multispectral optoacoustic tomography," Opt. Express, 18(19), 19592-19602 (2010).

[13] L. Li, R. J. Zemp, G. Lungu *et al.*, "Photoacoustic imaging of lacZ gene expression in vivo," J Biomed Opt, 12(2), 020504 (2007).

[14] D. Razansky, C. Vinegoni, and V. Ntziachristos, "Multispectral photoacoustic imaging of fluorochromes in small animals," Optics Letters, 32(19), 2891 (2007).

[15] D. Razansky, M. Distel, C. Vinegoni *et al.*, "Multispectral opto-acoustic tomography of deep-seated fluorescent proteins in vivo," Nat Photon, 3(7), 412-417 (2009).

[16] B. T. Cox, S. R. Arridge, and P. C. Beard, "Estimating chromophore distributions from multiwavelength photoacoustic images," Journal of the Optical Society of America a-Optics Image Science and Vision, 26(2), 443-455 (2009).

[17] D. Razansky, and V. Ntziachristos, "Hybrid photoacoustic fluorescence molecular tomography using finite-element-based inversion.," Med Phys, 34(11), 4293-301 (2007).

[18] A. Conjusteau, S. A. Ermilov, R. Su *et al.*, "Characterization of optoacoustic transducers through the analysis of angular-dependent frequency response," Proc. SPIE, 7177, 71770- 71778 (2009).

[19] R. Ma, A. Taruttis, V. Ntziachristos *et al.*, "Multispectral optoacoustic tomography (MSOT) scanner for whole-body small animal imaging," Optics Express, 17(24), 21414-21426 (2009).

[20] H. Zhang, K. Maslov, G. Stoica *et al.*, "Functional photoacoustic microscopy for high-resolution and noninvasive in vivo imaging.," Nat Biotechnol, 24(7), 848-51 (2006).

[21] P. Burgholzer, H. Grun, M. Haltmeier *et al.*, "Compensation of acoustic attenuation for high-resolution photoacoustic imaging with line detectors," Proc. SPIE, 6437, 643724-1 (2007).

[22] G. Golub, [Matrix computations] Johns Hopkins University Press, 3rd ed., Baltimore(1996).

[23] C. C. Paige, and M. A. Saunders, "LSQR: An Algorithm for Sparse Linear Equations and Sparse Least Squares," ACM Trans. Math. Softw., 8(1), 43-71 (1982).

[24] T. Jetzfellner, D. Razansky, A. Rosenthal *et al.*, "Performance of iterative optoacoustic tomography with experimental data," Applied Physics Letters, 95(1), - (2009).

[25] M. Schweiger, S. R. Arridge, M. Hiraoka *et al.*, "The finite element method for the propagation of light in scattering media: Boundary and source conditions," Medical Physics, 22(11), 1779-1792 (1995).

[26] W. Bangerth, R. Hartmann, and G. Kanschat, "deal. II - A general-purpose object-oriented finite element library," Acm Transactions on Mathematical Software, 33, (2007).